Probing the Interfacial Structure of Bilayer Plasma Polymer Films via Neutron Reflectometry

Yali Li, Andrew Nelson, Christopher D. Easton, David R. Nisbet, John S. Forsythe, Benjamin W. Muir*

Bilayer plasma polymer (PP) films were examined using a combination of X-ray and neutron reflectometery and X-ray photoelectron spectroscopy to gain an understanding of the interfacial structures that form between the films. Three different PP films were produced from the monomers hexamethyldisiloxane (HMDSO), di(ethylene glycol) dimethyl ether (DG), and allylamine (AA) at different load powers. These films were used as "substrates" for the subsequent deposition of a deuterated DG (dDG) PP top film. The width of the interfacial region was found to be strongly dependent on the chemical and physical properties of the substrate film. These findings have relevance to the general use and application of plasma polymer films.

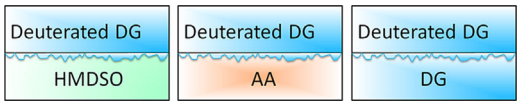

1. Introduction

The ability to selectively modify a surface is useful in numerous applications, including optical components, electronics, renewable energy systems (solar cell, fuel cells), and medical implants.[1–4] The use of plasma for controlled surface modifications of various substrate materials has advanced rapidly over the last few decades and continues to grow.[5–7] However, there is still a lack of understanding of the chemical and physical properties required of a particular substrate material (be that organic or inorganic) to ensure an optimal coating with a plasma polymer film of choice is stable and adherent. Therefore, study of the interface region that forms between a substrate and its plasma polymer are of particular interest. Herein we report an investigation probing the interface region that forms between various plasma polymers used as "substrate" materials for the coating with a deuterated plasma polymer top coat film.

The plasma polymerization of monomers such as HMDSO, DG, and AA films are well known.[8–12] HMDSO plasma polymer films are rich in Si (organosilicone films) and provide good optical barrier and mechanical properties which have been used extensively in microelectronics and other applications.[13] The DG monomer contains ether functional groups, where the concentration of residual ether units in a PP film can be controlled via the deposition conditions. This allows the protein resistant properties of a DG surface to be tuned.[14,15] PP films generated from AA retain reactive amine, imine, and nitrile functionalities that

Dr. Y. Li, Dr. C. D. Easton, Dr. B. W. Muir
CSIRO Manufacturing Flagship, Clayton South, VIC 3169, Australia
E-mail: ben.muir@csiro.au
Dr. Y. Li, Prof. J. S. Forsythe
Department of Materials Engineering, Monash University, Clayton, VIC 3168, Australia
Dr. A. Nelson
Bragg Institute, Australian Nuclear Science and Technology Organisation (ANSTO), Locked Bag 2001, Kirrawee DC, NSW 2232, Australia
NIST Center for Neutron Research, National Institute of Standards and Technology, Gaithersburg 20899, Maryland, USA
Dr. D. R. Nisbet
College of Engineering and Computer Science, The Australian National University, Acton, ACT 2601, Australia

DOI: 10.1002/ppap.201500158

are useful as supports for further grafting reactions, especially in the biomedical science arena.[16–18]

Although single layer plasma polymer films hold enormous promise for a range of applications, what actually occurs at the interface between a PP and its substrate is not well understood. It is typically believed that a range of fragmentation, recombination, and radical crosslinking reactions can occur, which anchor a PP film to its substrate.[19] The effect that the substrate type (metal, polymeric, or ceramic, etc), its surface chemistry, and physical properties have on the adhesion and properties of the PP film at the interface are largely unknown. Problems of adhesion are typically addressed by an empirical process.[20] The key for further advancement in the field lies in deepening our understanding of a PP film's physical and chemical properties and how the plasma polymerization process is affected by the substrate material, the monomer chemistry, and the deposition conditions. Various analytical methods have been employed to fully elucidate the chemical composition of plasma polymer films, such as FTIR, XPS, NEXAFS, and TOF-SIMS but few can provide information about the interface of a PP film with its substrate.[21–24] To investigate a PP's film thickness and structure at a surface the most commonly used techniques are ellipsometry and AFM.[10,25] In addition to these methods, it is also desirable to probe the internal structure of bulk films and interface mixing of multilayered PP coatings.

One method used to visualize a PP interface is viewing sectioned multilayer samples with Scanning Force Microscopy (SFM). Zhang et al. examined HMDSO films deposited under alternating plasma conditions. The difference in mechanical contrast within each PP layer allowed analysis of the interface and an estimation of the PP films roughness.[26] Cech and co-workers used a similar methodology to investigate hydrogenated amorphous carbon–silicon (a-SiC:H) multilayer films.[27] With this technique, one drawback is that the sectioned surface may contain artifacts due to smearing of the interface. Another limitation with this approach is that individual PP layers need to be relatively thick in order to avoid interference from surrounding layers.

A non-destructive method for thin film analysis is a combination of X-ray and Neutron Reflectometry (XRR, NR). XRR and NR are sensitive to nanoscale sub-surface structures and allow the determination of the full chemical composition of PP films (in concert with information obtained with XPS).[28] Reflectometry techniques require that the PP films be flat, smooth, and deposited onto flat substrates, such as polished silicon wafers. Neutron reflection methods are especially advantageous for multilayer films in which one layer is made from deuterated monomers. Hydrogen and deuterium have radically different scattering lengths ($H = -3.74 \times 10^{-15}$ m, $D = 6.67 \times 10^{-15}$ m), and the difference means that deuterated films scatter more strongly, making it easier to distinguish individual layers within a multilayer.[29] Our group has already used NR to study HMDSO (10 W),[30] AA (20 W),[28] DG (10, 20 and 50 W)[31] PP single layer films. Previous NR studies by other groups have focused on the density profiles and swelling behavior of plasma polymerized methylmethacrylate,[32] octafluorocyclobutane (OFCB),[33] and benzene[34] films. Only the work of Kim et al. has used XRR and NR to explore both single and multilayered plasma polymer films.[35] OFCB and deuterated benzene were used as starting monomers to produce single and bilayer PP films. They found that the interface of the bilayer was significantly rougher than that of the film-air interface of single layer films and they argued that it is a result of reactive plasma chemistry occurring locally at the interface.

We hypothesized that studying multi layer PP films would allow us to gain an insight into the interfacial properties of the films. First we created substrate PP films of controlled thickness from HMDSO (10 and 20 W), DG (20 and 40 W), and AA (20 and 40 W) monomers. We then subjected those substrate films to a second capping layer of 20 W dDG PP. Use of deuterated DG as the top film increases contrast between the two layers; it also shows negligible changes in chemistry as it ages. The interfacial structures were determined using XRR and NR before, and after, the capping layer was added. The surface chemistry of the PP films was characterized using XPS. The stoichiometric composition and mass densities of the PP films were obtained by modeling and combining the XPS, XRR, and NR data.

2. Experimental Section

2.1. Sample Preparation

Ultra-flat single crystal, silicon wafers (<111>, 100 mm diameter, 10 mm thick, *Silrec Corporation*, San Jose and <100>, 100 mm^2 × 0.5 mm thick, from M.M.R.C Pty Ltd, Melbourne Australia) were used as substrates for the deposition of plasma polymer thin films. All wafers were cleaned immediately prior to plasma polymer deposition by ultrasonication in a surfactant solution of 2% ethanol with 2% RBS-35 (Pierce, U.S.A) for 1 h, followed by rinsing with copious amount of MilliQ water and finally dried in a high-pressure stream of nitrogen. The large wafers were used for reflectometry measurements and the smaller wafers were used as substrates for XPS characterization. Plasma deposition on the large and small wafers was performed simultaneously (small wafers were placed around the edge of the large wafer).

The monomers HMDSO (Sigma–Aldrich, NMR grade, 99.5%), DG (BDH, 99%), AA (Sigma–Aldrich, 98%), and dDG (Cambridge Isotope Laboratories, Inc. U.S.A. 98%) were all used without further purification.

2.2. Plasma Polymerization

Deposition of HMDSO, DG, and dDG plasma polymer films were carried out in a custom-built reactor. Briefly, a cylindrical reactor

chamber is used, with a height of 350 mm and a diameter of 170 mm. Within this chamber sit two capacitively coupled electrodes, spaced 100 mm apart. The top electrode ($d = 95$ mm) was connected to a RF power supply, while the bottom electrode ($d = 140$ mm) was grounded. The AA plasma polymerization reactor consists of a chamber of same size and fitted with two circular electrodes of 103 mm in diameter, spaced 150 mm apart. Clean wafers were placed on the lower electrode and a continuous radio frequency glow discharge (RFGD) was generated at the upper electrode. The monomer vapors were supplied to the reactor chamber from the liquid reagents in a round-bottom flask via a stainless steel line and a manual valve for fine control of the flow. HMDSO, DG, and dDG monomer flasks were kept in ambient air, while a highly volatile AA monomer flask was cooled in iced water, during experiments. All monomer liquid was degassed before plasma deposition.

The plasma polymerization parameters of the four monomers were selected such that films of appropriate thicknesses for reflectivity measurements were produced. The plasma deposition of HMDSO films was performed using a frequency of 200 kHz, load powers of 10 and 20 W, and initial monomer pressure of 10 Pa for a treatment time of 8 (final pressure 13 Pa) and 5 (final pressure 15 Pa) seconds, respectively. Similarly, deposition conditions for DG were at a frequency of 125 kHz, load powers of 20 and 40 W with initial monomer pressure of 20 Pa for a treatment time of 14 (final pressure 41 Pa) and 8 (final pressure 52 Pa) seconds, respectively. The parameters chosen for AA were at a frequency of 200 kHz, load powers of 20 and 40 W with initial monomer pressure of 20 Pa for a treatment time of 17 (final pressure 37 Pa) and 10 (final pressure 42 Pa) seconds, respectively. Six single layer plasma polymer films were produced using the above conditions; another six samples were made under identical conditions, then subjected to an additional dDG plasma polymerization process. The dDG layer was formed under a frequency of 125 kHz and a load power of 20 W with initial monomer pressure of 20 Pa for a treatment time of 16 s, and the final pressure is 40 Pa. Prior to deposition, the reactor was evacuated to a base pressure of 0.1 Pa. After deposition, the reactor was immediately pumped down to base pressure before venting. The samples were stored in clean petri dishes under ambient conditions until further analysis. For simplicity, a sample name of "HM10" indicates that the film was deposited using HMDSO monomer vapor and 10 W load power; "HM10D" indicates that HM10 was further treated with dDG 20 W plasma polymerization.

2.3. X-Ray Photoelectron Spectroscopy (XPS)

XPS analysis was performed using an AXIS HSi spectrometer (Kratos Analytical Ltd, U.K.) equipped with a monochromated Al-K_α X-ray source at a power of 144 W (12 mA, 12 kV). All elements presented were identified from low resolution survey spectra (acquired at a pass energy of 160 eV). The atomic concentrations of the detected elements were calculated using integral peak intensities and the sensitivity factors supplied by the manufacturer. In addition, high resolution C 1s spectra were obtained at a pass energy of 40 eV yielding a typical peak width (full width at half maximum) of 1.0–1.1 eV for polymers. Samples were measured first in the as-deposited state and then at the time of reflectometry measurements to account for aging changes in the chemistry of the plasma polymer film.

2.4. Neutron and X-Ray Reflectometry

Neutron and x-ray reflectometry data were collected at the NIST Center for Neutron Research, National Institute for Standards and Technology, Gaithersburg. XRR data were collected using a Bruker diffractometer ($\lambda = 1.5406$ Å). NR data were collected on the *Magik* horizontal scattering plane reflectometer.[29] In both cases the reflectivity, i.e., the ratio of specularly reflected intensity to incident beam intensity, was measured as a function of momentum transfer, Q. Momentum transfer is given by the relation $= {}^{4\pi}/_{\lambda}\sin\Omega$, where λ is the wavelength of incident radiation and Ω is the angle of incidence of the incoming beam. Additional NR measurements were performed on the *Platypus* reflectometer at the Australian Nuclear Science and Technology Organisation.[36] The reflectometry data were analyzed using a standard least squares method in the *Motofit* program,[37] weighting data on a logarithmic scale and using the instrumental resolution functions.

3. Results and Discussion

3.1. Surface Chemistry

One of the challenges when working with PP's is the tendency of some films to gradually age over time upon exposure to atmosphere. This is primarily due to post oxidation reactions within the films from residual radicals.[38,39] We allowed for the possible change in surface chemistry of the film over time by analyzing samples via XPS immediately after deposition and at the time of NR and XRR measurements. The XPS derived elemental analysis of the single layer PP films (in atomic%), at the time of NR and XRR measurements, is presented in Figure 1 and Table 1. Compared to the freshly deposited films (Table S1a), the HMDSO and AA films exhibit signs of oxygen incorporation with increases of approximately 1 at.%, while the DG films do not appear to oxidize. For the DG and AA PP films, low levels of silicon are also detected. This is likely due to the placement of the XPS samples on the outer most region of the 10 cm diameter silicon block, towards the edges of the lower plasma reactor electrode; the XPS samples were placed in this position to avoid disruption of the center of the film used for NR measurements (schematic S1). We have noted that the PP films deposited on these large silicon blocks are slightly thinner than films deposited onto standard 0.5 mm thick silicon wafers using the same electrode under the exact same plasma deposition conditions. The thinner PP films are close to the detection limit of XPS ($\sim$<100 Å), hence a small contribution from the substrate and/or a trace amount of Si contamination is observed. Both the 10 and 20 W deposited HMDSO PP films are rich in oxygen and silicon when compared to the

DOI: 10.1002/ppap.201500158

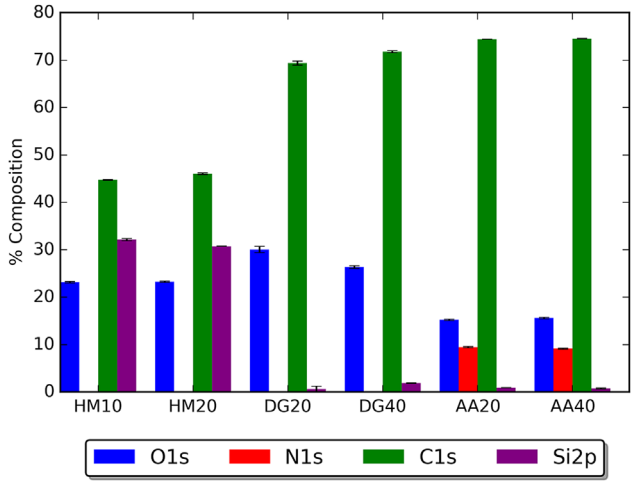

Figure 1. Elemental composition (atomic%) of the single layer plasma polymers made from HMDSO, AA and DG derived from XPS survey spectra for films produced at 10, 20, or 40 W load powers. The error bars display the standard deviation of the measurements ($n = 2$).

HMDSO monomer while the carbon content (e.g, for 10 W film, O/C = 0.51, Si/C = 0.70) reduced dramatically in contrast to the starting monomer (O/C = 0.17, Si/C = 0.33). The well-established mechanism for this phenomenon is that during the plasma polymerization of HMDSO, methyl abstraction is the major fragmentation and activation pathway in the RFGD whilst scission of Si—O bonds occurs to a much lesser extent.[30,39,40]

For the AA PP films, the main elemental components of the films are carbon, nitrogen and oxygen. The carbon content differs slightly from the monomer, but the nitrogen content is less than half that of the AA monomer. The drop in nitrogen content relative to the starting monomer in the films is typical of amine functional plasma polymer systems such as these. The oxygen incorporation originates from residual oxygen gas and water vapor residues in the reactor chamber and post plasma deposition oxidation reactions upon exposure to the atmosphere. We note that the oxygen content in these films is slightly higher than compared to such films previously reported in the literature.[17,28,41]

For the DG PP films, the elemental analysis from XPS reveals films that consist predominantly of carbon and oxygen. The O/C for the 20 W deposited DG PP films are similar to our previous studies,[9,31,42] however the O/C was greater by 1.7% for the 40 W DG PP compared to our previous results. We believe that this is due to the shorter deposition times (8 s vs. >15 s) employed in the current study. The RFGD in the initial stages of plasma deposition is less energetic, as evidenced visually by a weaker intensity plasma glow discharge. Therefore, in the initial stages of film deposition there are fewer molecular dissociation and scission events of the gaseous monomer. As the plasma deposition time increases, the RFGD reaches equilibrium and the resultant surface chemistry does not change significantly with extended deposition times. The time dependant change in the substrate temperature during plasma deposition may also account for this slight discrepancy in the O/C in the 40 W DG PP film.

The XPS analysis of the top dDG PP layer in the bilayer samples are summarized in Table 1. The dDG layers deposited on top of the single layer "substrate" PP films are formed under fixed process parameters and display minimal variation in the carbon and oxygen ratios across the six samples. As expected the dDG PP topcoat and the DG 20 W PP substrate film possess similar O/C ratios. The dDG films are stable after 1 week of storage (Table S1). Analysis of the C1s spectra of all six dDG20 layers (Figure 2) reveals that they display similar bonding environments, which consist of two major components: hydrocarbon bonds (285 eV) and C—O bonds (286.5 eV). It is reasonable to infer that the plasma environment produced in the top coat dDG20 plasma polymerization is consistent across the range of different PP substrate films. Overlaying a dDG20 (top coat) spectrum with a DG20 (substrate) spectrum (Figure 2c), minor differences in the distribution of peak intensity can be observed. This could be attributed to the presence of deuterium in replacement of hydrogen, which may contribute to subtle changes in the dissociation of chemical bonds and recombination processes during PP deposition or differences resulting from differential charging of the sample during XPS analysis.

3.2. Characterization of Films by XRR and NR

The air-solid NR data from both single layer PP films and bilayer films are shown in Figure 3, while the structural parameters of each film are summarized in Table 2. The corresponding XRR data and model parameters are given in the supporting information (Figure S1 and Table S2). The NR curves differ most notably in the fringe period (related to layer thickness) and fringe amplitude (related to change of scattering length density (SLD) across an interface). The data from the thicker bilayer films contain more fringes with a smaller spacing when compared to the data from single layer films. The model SLD profiles corresponding to each of the fits are shown in the inset of Figure 3. The SLD obtained for the PP films in this study are similar to those reported in the literature.[28,30,31]

For the single layer HMDSO, AA, and DG PP films the structural model consists of a thin transition layer between the silicon substrate and the layer describing the majority of the PP film, except for the HM10 PP which can be described by a single layer. The remainder of the film (for all PP) possesses a uniform SLD and is very smooth at the air-film

Table 1. Elemental composition (atomic% and atomic ratios) derived from XPS survey spectra of the various PP films studied in this work. Presented are the mean values with standard deviation ($n = 2$). A sample name of "HM10" indicates that the film was deposited using HMDSO as a monomer vapor and a 10 W load power. In addition, "HM10D" represents the bilayer film whereby HM10 was further treated with a dDG 20 W plasma polymerization. The same nomenclature applies for all of the films listed below where D is the bilayer film with a dDG 20 W plasma polymer film on top of the underlying "substrate" PP film.

Atomic %	**O 1s**	**N 1s**	**C 1s**	**Si 2p**
HM10	23.17 ± 0.16	–	44.72 ± 0.08	32.11 ± 0.24
HM10D	28.66 ± 0.16	–	70.52 ± 0.05	0.83 ± 0.11
HM20	23.25 ± 0.13	–	46.02 ± 0.16	30.73 ± 0.01
HM20D	29.23 ± 0.28	–	69.86 ± 0.40	0.93 ± 0.13
DG20	30.04 ± 0.66	–	69.37 ± 0.55	0.60 ± 0.11
DG20D	28.61 ± 0.04	–	71.39 ± 0.04	–
DG40	26.35 ± 0.29	–	71.79 ± 0.23	1.86 ± 0.06
DG40D	28.77 ± 0.27	–	71.21 ± 0.27	0.02 ± 0.01
AA20	15.21 ± 0.13	9.48 ± 0.13	74.43 ± 0.03	0.89 ± 0.02
AA20D	28.95 ± 0.11	–	70.96 ± 0.04	0.10 ± 0.13
AA40	15.60 ± 0.16	9.14 ± 0.11	74.53 ± 0.04	0.74 ± 0.10
AA40D	28.34 ± 0.28	–	71.57 ± 0.28	0.10 ± 0.00
Atomic ratios	O/C	N/C	Si/C	
HM10	0.52	–	0.72	
HM10D	0.41	–	0.01	
HM20	0.51	–	0.67	
HM20D	0.42	–	0.01	
DG20	0.43	–	0.01	
DG20D	0.40	–	–	
DG40	0.37	–	0.03	
DG40D	0.40	–	–	
AA20	0.20	0.13	0.01	
AA20D	0.41	–	–	
AA40	0.21	0.12	0.01	
AA40D	0.40	–	–	

interface. The data shows (Table 2) that higher load powers lead to rougher films, with a two fold increase in roughness. In *Motofit* the interfacial roughness is Gaussian, i.e., the SLD profile between two layers can be described using the Error function. The roughness parameter describes the standard deviation of the parent Gaussian distribution of the Error function for a particular interface. This phenomenon may be in part due to larger clusters of molecules recombining in the plasma glow discharge during film growth which has been shown to result in rougher surfaces and interfaces.[43]

For the bilayer PP films, a two layer model was adequate for all datasets. This model includes the deuterated DG PP layer (layer 1) and the underlying PP film (layer 2). In this model, the roughness of layer 2 represents the extent of the interfacial mixing between the two PP films that make up the bilayer. Comparing air-film interface roughness values, the value is consistently larger (with the exception of AA) for the sample fabricated at lower power than the corresponding sample deposited at higher power. It is evident from Table 2 that all the bilayer PP films possess an intermixing region that is much broader than the air-film roughness of the corresponding substrate film. For instance, the interfacial roughness of the HM10D bilayer (17.1 Å) is 8 × that of the HM10 single layer PP film (2.1 Å), while DG20D and AA20D have a 4 and 2.5-fold increase, respectively. That the amount of interfacial broadening is different for each of the different types of substrate indicates that there are differences in hardness and resistance to ablation for each

DOI: 10.1002/ppap.201500158

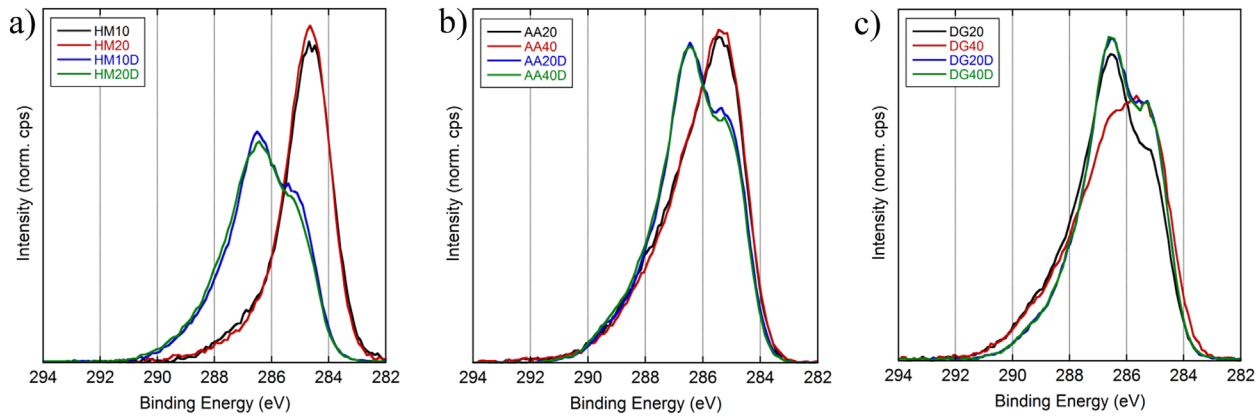

Figure 2. Overlay of selected, representative high-resolution C 1s spectra of a) HMDSO, b) AA, c) DG plasma polymer films, with their corresponding dDG bilayer PP films.

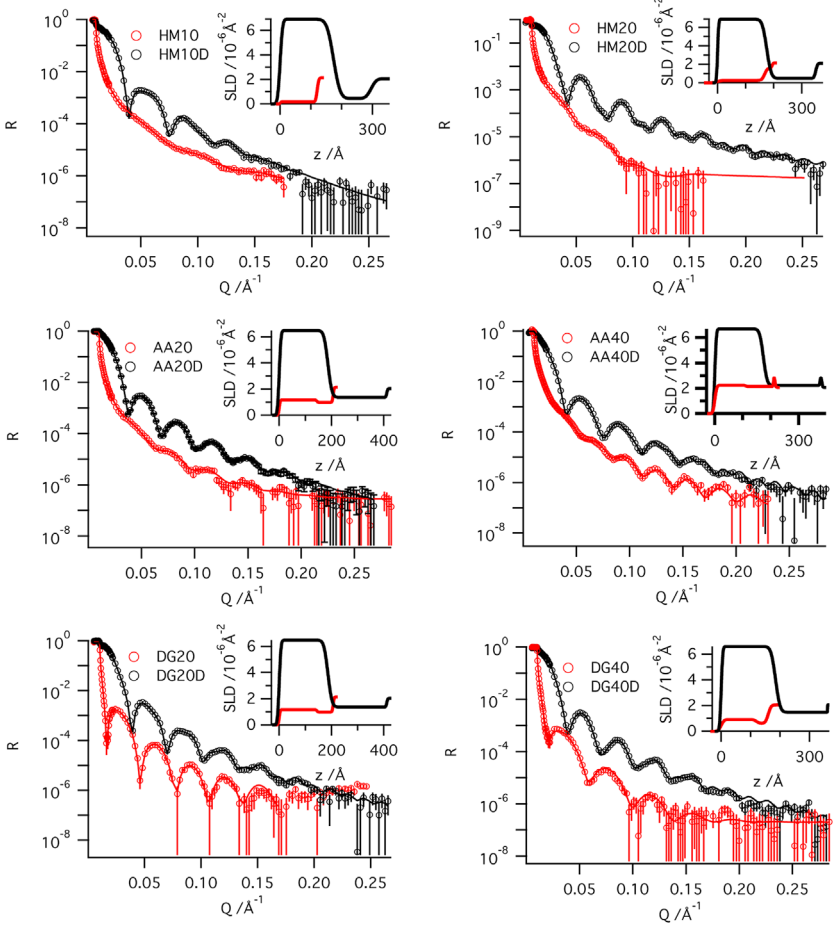

Figure 3. NR spectra from the air/plasma polymer film/silicon systems. Each subplot contains the spectra for single and bilayer films. The symbols represent the observed reflectivity data (error bars are ±1 standard deviation) while the solid lines are model fits to the data. The insets are the SLD profiles of the various PP films.

type of monomer used to deposit the substrate films, which we will discuss later. The ratio of the interfacial roughness at the bilayer-layer interface compared to the air-layer interface of the corresponding single layer PP film is shown in Figure 4. Figure 5 also shows a representation of this effect by plotting normalized interfacial SLD profiles for the bilayer plasma polymer interfaces compared to the plasma polymer substrate layers against air. It is clear from Figures 4 and 5 that the creation of the bilayer by deposition of the dDG20 PP top coat roughens and broadens the interface of the PP acting as a substrate. Furthermore the internal interface in bilayers whose substrate films were deposited at lower power broaden much more than those deposited at higher power. The reason for these changes will be discussed later.

The SLD of all six dDG20 top PP films are very similar, even though they are prepared from six individual PP depositions (Table 2). This shows the reproducibility is good when generating multiple PP films from individual depositions. The data shows that neutron reflectometry measurements are reliable for distinguishing small deviations in the properties of the multi layer PP films. The large SLD of the dDG20 PP film (average 6.67 × 10^6 Å^{-2}) compared with the DG20 PP film (1.17 × 10^6 Å^{-2}) is due to the larger scattering length of deuterium

Table 2. Film thickness, scattering length density, and roughness of single and bilayer PP films as used for NR model fitting. For ease of presentation we only show the values obtained for the NR models, the XRR models are given in Table S2. For the bilayer systems layer 1 represents the top deuterated DG layer, while layer 2 refers to the underlying base PP film. For the single layer systems it was possible to resolve two regions of slightly different SLD. Uncertainties are reported as 1 standard deviation.

NR	Thickness (Å)		SLD ($\times 10^6$ Å^{-2})		Roughness (Å)	
Single	**1**	**2**	**1**	**2**	**Air/1**	**1/2**
HM10	120.5 ± 1.0		0.17 ± 0.01		2.1 ± 1.3	
HM20	167.6 ± 2.6	26.6 ± 2.5	0.27 ± 0.01	1.61 ± 0.18	10.9 ± 2	8.2 ± 3.8
DG20	144.0 ± 1.6	62.3 ± 1.6	1.17 ± 0.01	0.99 ± 0.01	3.2 ± 1.0	2
DG40	106.7 ± 13.6	57.8 ± 1.2	0.94 ± 0.02	0.78 ± 0.32	11.1 ± 1.0	15.8 ± 5.0
AA20	163.9 ± 3.4	29.9 ± 6.0	1.95 ± 0.01	2.16 ± 0.03	4.9 ± 0.4	7.5 ± 2.1
AA40	110.4 ± 0.7	99.8 ± 0.2	2.25 ± 0.01	2.15 ± 0.01	5.6 ± 0.2	5.0 ± 1.2
Bilayer	1	2	1	2	Air/1	1/2
HM10D	173.4 ± 0.2	122.4 ± 0.5	6.92 ± 0.04	0.45 ± 0.04	6.4 ± 0.1	17.1 ± 0.2
HM20D	174.9 ± 0.1	178.5 ± 1.3	6.77 ± 0.04	0.48 ± 0.03	3.2 ± 0.1	12.7 ± 0.1
DG20D	186.2 ± 0.1	225.3 ± 0.5	6.47 ± 0.02	1.33 ± 0.02	5.5 ± 0.1	12.3 ± 0.1
DG40D	184.5 ± 0.1	176.0 ± 0.4	6.58 ± 0.02	1.53 ± 0.02	4.1 ± 0.1	11.9 ± 0.1
AA20D	189.5 ± 0.2	171.2 ± 4.6	6.59 ± 0.03	1.98 ± 0.05	4.9 ± 0.1	11.8 ± 0.2
AA40D	173.6 ± 0.2	216.5 ± 4.8	6.67 ± 0.05	2.24 ± 0.07	4.4 ± 0.1	10.7 ± 0.2

compared to hydrogen, as the other two elements (C/O) in the film are at the same concentration. One parameter that does change amongst the dDG20 films are their roughness values. Aside from the HM20D PP bilayer film, the other dDG20 top coat films have an air-film interface that is rougher than the single layer DG20 PP film (3.2 Å). We hypothesize that the increase in roughness of the second layer is related to the surface morphology of the substrate; in the case of the dDG20 top PP films this is the "substrate"

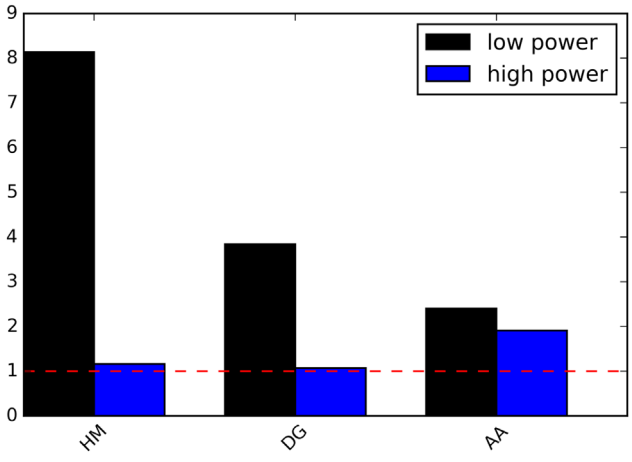

Figure 4. The ratio between the bilayer interface roughness and the roughness of the corresponding substrate film.

PP film rather than a smooth silicon wafer. The base PP films have their own inherent surface roughness and chemistries that are further modified during the second plasma polymerization process. This leads to varied surface roughnesses. When the dDG20 layer grows from the underlying PP film interface, it will be expected to replicate the underlying films surface morphology. The increase in dDG20 roughness also depends on the degree of broadening of the underlying interface, i.e., films made at the lower load power which possess a greater broadening at the bilayer interface, result in the generation of a rougher top layer. We hypothesize that deposition of the second plasma polymer layer also causes ablation of the first PP film, roughening the interface between the two films and subsequently affects the roughness of the air interface of the dDG20 PP film.

It is important to elucidate the cause of the observed differences in the interfacial structure of the various bilayer films. The plasma polymerization load power plays a critical role in determining the degree of unsaturation and/or crosslinking within a PP film. To deduce the reasons for why the interfacial roughness doesn't broaden as much in higher power PP films, we need to know more about the film composition than that provided by XPS alone. We calculate the full atomic composition of the films by simultaneously fitting the composition and mass densities to the average x-ray and neutron SLD values determined from the *Motofit*

DOI: 10.1002/ppap.201500158

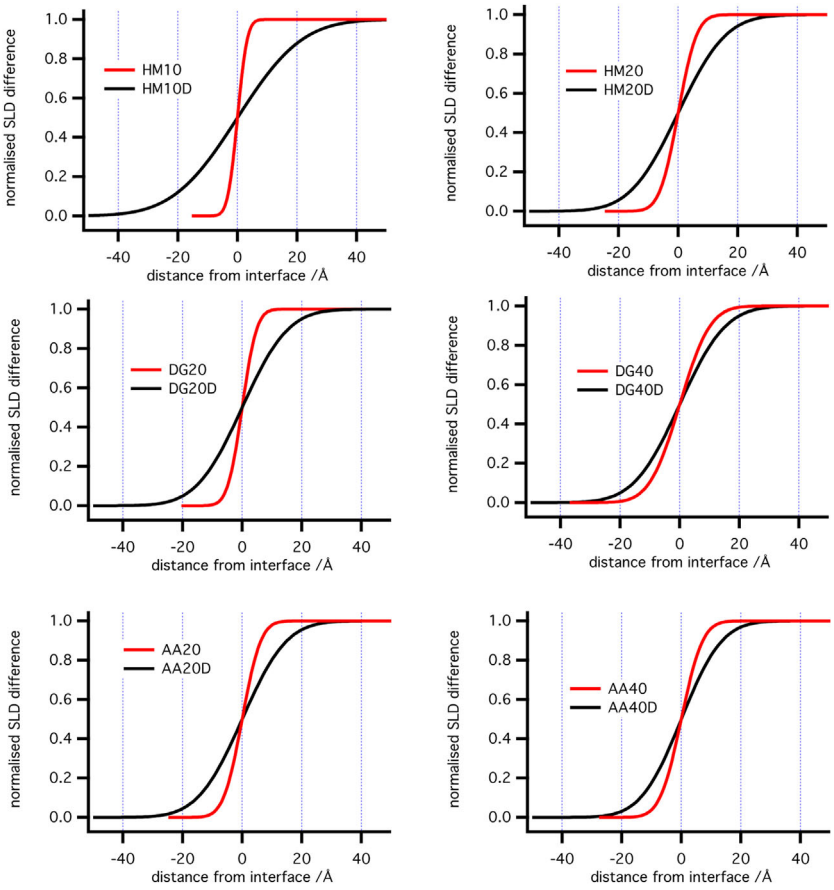

Figure 5. Normalized interfacial scattering length density profiles for the DG/PPx interface (e.g., HM10D) compared to that of the PPx/air interface. Deposition of the overlying DG film roughens the interface it is deposited on, which is magnified if the substrate plasma polymer is deposited at a lower power.

model along with the XPS results.[28] The assumption in these calculations is that the surface composition (atomic%) determined by XPS is also an accurate representation of the bulk composition, and that there are no voids in the sample. The estimated full atomic composition and the film mass density are shown in Table 3. Consider the DG PP films first. From the structural data in Table 3 (the degree of unsaturation based on the Empirical formula composition) and the XPS C1s spectra (greater hydrocarbon contribution) in Figure 2, it is evident that the DG40 PP film contains more hydrocarbon and less ether units compared to the DG20 PP film. The mass density of more highly crosslinked films is also expected to be lower than films with less crosslinks, as observed. This data indicates that the DG40 PP film is more unsaturated and is consistent with previous reports by us on these films.[31] For the HMDSO and AA PP films, the XPS high resolution C 1s spectra (Figure 2) do not provide information on their degree of unsaturation, as the overlay of the spectra are of identical shape.

The mass densities for the AA PP's at the two different load powers are the same but their compositions differ somewhat in terms of their hydrogen content (Table 3) indicating the lower power AA PP film is less unsaturated than the higher power AA PP film. The density of the HMDSO higher power film is 1.25 g cm^{-3} while the lower power film is 1.05 g cm^{-3}. The elemental compositions of the high and low power films are similar, but the higher power film has slightly less Si and H that also indicates a higher level of unsaturation. Interestingly, the film density and plasma glow discharge load power correlation seen in the HMDSO PP films is the opposite of what was observed in the DG PP system (lower power = higher mass density), but is consistent with our previous reports on HMDSO and DG PP's.[30,31] The significant difference in the HMDSO bilayer broadening between the high and low power depositions can therefore be attributed to a significantly greater mass density and a higher degree of unsaturation/crosslinking for the high power film, which would result in less ablation/mixing during deposition of the dDG PP topcoat film.

Since the bond energies of unsaturated bonds are significantly higher than those of single bonds (C—C 346, C—O 358, C=C 839l, and C=O 1072 Kj/mol), a substrate film with lower crosslinking and more unsaturation will be expected to undergo a larger degree of fragmentation when exposed to a subsequent plasma glow discharge. Therefore, the films that contain more single bonds (the lower power films) would etch to a larger extent when compared to more unsaturated films (higher power), resulting in a rougher and broader bilayer interface.

To compare the chemical composition and density of the substrate film after deposition of the dDG topcoat we have to assume that the XPS derived empirical composition of the heavier elements (C/N/O/Si) does not change. Table 3 shows that the density of the substrate film does not show significant change after the dDG topcoat is deposited. However, the hydrogen content for both the DG and HM substrate films appear to decrease significantly; the SLD values for layer 2 (Table 2) get slightly larger when the dDG topcoat is deposited (e.g., SLD HM20_layer 1 = 0.27 vs. HM20D_layer2 = 0.48). The likely reason why the SLD's increase is because deuterium atoms are implanting themselves in the substrate PP films structure through ablation, recombination and deposition during the RFGD of the dDG topcoat . This manifests as lower hydrogen atom ratios in the calculated values in Table 3. In contrast, the AA

Table 3. Mass density and composition of all single and bilayer PP films as determined by XRR and NR reflectometry in combination with XPS elemental composition. The theoretical monomer compositions are shown for comparison.

Single layer	Composition		Mass density (g cm^{-3})	
HM monomer	**$C_1O_{0.17}Si_{0.33}H_3$**		–	
HM10		$C_1O_{0.51}Si_{0.70}H_{3.02}$		1.06
HM20		$C_1O_{0.52}Si_{0.64}H_{2.89}$		1.25
DG monomer	**$C_1O_{0.5}H_{2.33}$**		–	
DG20		$C_1O_{0.43}H_{1.61}$		1.29
DG40		$C_1O_{0.36}H_{1.56}$		1.03
AA monomer	**$C_1N_{0.33}H_{0.33}$**		–	
AA20		$C_1N_{0.13}O_{0.20}H_{1.23}$		1.34
AA40		$C_1N_{0.12}O_{0.21}H_{1.06}$		1.35
Bilayer	Layer 1	Layer 2	Layer 1	Layer 2
HM10D	$C_1O_{0.41}D_{1.07}$	$C_1O_{0.52}Si_{0.70}H_{2.58}$	1.47	1.11
HM20D	$C_1O_{0.42}D_{1.15}$	$C_1O_{0.51}Si_{0.63}H_{2.55}$	1.42	1.21
DG20D	$C_1O_{0.40}D_{1.12}$	$C_1O_{0.43}H_{1.56}$	1.35	1.36
DG40D	$C_1O_{0.40}D_{1.01}$	$C_1O_{0.37}H_{1.17}$	1.42	1.09
AA20D	$C_1O_{0.41}D_{0.94}$	$C_1N_{0.13}O_{0.20}H_{1.25}$	1.46	1.46
AA40D	$C_1O_{0.40}D_{1.05}$	$C_1N_{0.12}O_{0.21}H_{1.09}$	1.41	1.36

substrate composition does not change; it presents a greater resistance to ablation from reactive plasma species. This is a consequence of its higher mass density, which also manifests in a diminished interfacial film broadening compared to the other plasma polymers.

4. Conclusion

An investigation of the surface chemistry of plasma deposited AA, DG, and HMSDO thin films deposited at two load powers, with and without a deuterated diglyme top coat PP film was conducted. These bilayer plasma polymer systems were analyzed by a combination of complementary surface analytical methods which revealed that the resulting interfacial film structures are strongly reliant on the "substrate" plasma polymer films chemistries, differing significantly with the class of monomer used. We were able to accurately determine the structure of bilayer plasma polymer films and the full elemental composition and mass density of the film. All films showed a correlation between the degree of unsaturation in the substrate plasma polymer and the deposition power. The extent to which the bilayer interface is broadened is inversely correlated with the degree of unsaturation/deposition power; unsaturated/crosslinked films are more robust when the topcoat is applied. This finding is of note for researchers in the plasma polymer field when considering the substrate material of choice, the deposition conditions, and intended application for a particular plasma polymer system since it affects the adhesion and stability of the interface which forms.

Acknowledgements: We acknowledge the support of the National Institute of Standards and Technology, U.S. Department of Commerce, in providing the neutron research facilities used in this work. DN was supported by an NHMRC Career Development Fellowship, APP1050684. The identification of any commercial product or trade name does not imply endorsement or recommendation by the National Institute of Standards and Technology.

Supporting Information is available at Wiley Online Library or from the author.

Received: August 20, 2015; Revised: October 4, 2015; Accepted: October 5, 2015; DOI: 10.1002/ppap.201500158

Keywords: allylamine; hexamethyldisiloxane; interfaces; neutron reflectometry; plasma polymerization

[1] P. M. Martin, *Multifunctional Surface Engineering Applications*. John Wiley & Sons Inc., Hoboken, NJ, USA **2011**, p. 457.
[2] A. Biswas, I. S. Bayer, A. S. Biris, T. Wang, E. Dervishi, F. Faupel, *Adv. Colloid Interfac. Sci.* **2012**, *170*, 2.

DOI: 10.1002/ppap.201500158

[3] W.-J. Yoon, D. Bhattacharyya, R. B. Timmons, P. R. Berger, *Org. Electron.* **2010**, *11*, 1767.
[4] R. P. Patel, D. Chiavetta, C. A. Wolden, *J. Vac. Sci. Technol.* **2011**, *29*, 061508.
[5] H. Yasuda, M. Gazicki, *Biomaterials* **1982**, *3*, 68.
[6] H. Biederman, D. Slavínská, *Surf. Coat. Technol.* **2000**, *125*, 371.
[7] T. Desmet, R. Morent, N. D. Geyter, C. Leys, E. Schacht, P. Dubruel, *Biomacromolecules* **2009**, *10*, 2351.
[8] M. Bonnar, J. Wilson, B. Burnside, *J. Mater.* **1998**, *33*, 4843.
[9] B. W. Muir, A. Tarasova, T. R. Gengenbach, D. J. Menzies, L. Meagher, F. Rovere, A. Fairbrother, K. M. McLean, P. G. Hartley, *Langmuir* **2008**, *24*, 3828.
[10] Q. Cheng, K. Komvopoulos, *J. Phys. Chem. C.* **2008**, *113*, 213.
[11] K. Vasilev, A. Michelmore, P. Martinek, J. Chan, V. Sah, H. J. Griesser, R. D. Short, *Plasm. Process. Polym.* **2010**, *7*, 824.
[12] L. Denis, D. Cossement, T. Godfroid, F. Renaux, C. Bittencourt, R. Snyders, M. Hecq, *Plasm. Process. Polym.* **2009**, *6*, 199.
[13] J. Tyczkowski, Eelectrical and optical properties of plasma polymers, in *Plasma Polymer Films*, Imperial College Press/ World Scientific Publishing Co., **2004**, p. 143.
[14] N. P. Reynolds, K. E. Styan, C. D. Easton, Y. Li, L. Waddington, C. Lara, J. S. Forsythe, R. Mezzenga, P. G. Hartley, B. W. Muir, *Biomacromolecules* **2013**, *14*, 2305.
[15] C. Choi, D. Jung, D. W. Moon, T. G. Lee, *Surface and Interface Analysis* **2011**, *43*, 331.
[16] J. B. Alison, C. Sennur, D. S. Robert, G. Alec, J. B. Nick St, *J. Phys. Chem. B.* **2001**, 105.
[17] L. H. Andrew, T. Helmut, Q. Jamie, H. V. Nicolas, *Surf. Sci.* **2008**, 602.
[18] E. R. David, E. S. Louise, A. S. David, D. S. Robert, D. W. Jason, *Biomater. Sci.* **2014**, *2*, 875.
[19] H. K. Yasuda, Competitive ablation and polymerization (CAP) mechanisms of glow discharge polymerization, in *Plasma Polymerization*, ACS Symposium Series, Vol. *108*, American Chemical Society **1979**, chapter 2, p. 37.
[20] K. Vasilev, A. Michelmore, H. J. Griesser, R. D. Short, *Chem. Commun.* **2009**, *24*, 3600.
[21] W. E. S. Unger, S. Swaraj, U. Oran, A. Lippitz, *Surf. Interface Anal.* **2006**, *38*, 522.
[22] S. Swaraj, U. Oran, J. F. Friedrich, A. Lippitz, W. E. S. Unger, *Plasm. Process. Polym.* **2007**, *4*, 376.
[23] I. Retzko, J. F. Friedrich, A. Lippitz, W. E. S. Unger, *J. Electron Spectrosc. R. Phenom.* **2001**, *121*, 111.
[24] A. G. Shard, J. D. Whittle, A. J. Beck, P. N. Brookes, N. A. Bullett, R. A. Talib, A. Mistry, D. Barton, S. L. McArthur, *J. Phys. Chem. B.* **2004**, *108*, 12472.
[25] S. Sharma, R. W. Johnson, T. A. Desai, *Biosens. Bioelectron.* **2004**, *20*, 227.
[26] Y. Zhang, J. Arfsten, S. Pihan, T. Kaule, R. Förch, R. Berger, *J. Colloid Interface Sci.* **2010**, *351*, 532.
[27] C. Vladimir, T. Rutul, S. David, *Plasm. Process. Polym.* **2011**, *8*, 1107.
[28] B. W. Muir, A. Nelson, A. Fairbrother, C. Fong, P. G. Hartley, M. James, K. M. McLean, *Plasm. Process. Polym.* **2007**, *4*, 433.
[29] J. A. Dura, D. J. Pierce, C. F. Majkrzak, N. C. Maliszewskyj, D. J. McGillivray, M. Lösche, K. V. O'Donovan, M. Mihailescu, U. Perez-Salas, D. L. Worcester, S. H. White, *Rev. Sci. Instrum.* **2006**, *77*.
[30] A. Nelson, B. W. Muir, J. Oldham, C. Fong, K. M. McLean, P. G. Hartley, S. K. Øiseth, M. James, *Langmuir* **2005**, *22*, 453.
[31] D. J. Menzies, A. Nelson, H.-H. Shen, K. M. McLean, J. S. Forsythe, T. Gengenbach, C. Fong, B. W. Muir, *J. Roy. Soc. Interface.* **2012**, *9*, 1008.
[32] H. S. Jeon, J. Wyatt, D. Harper-Nixon, D. H. Weinkauf, *J. Polym. Sci. B* **2004**, *42*, 2522.
[33] S. Peri, B. Akgun, S. Satija, H. Jiang, J. Enlow, T. Bunning, M. Foster, *ACS Appl. Mater. Interface.* **2011**, *3*, 3375.
[34] R. P. Someswara, H. Brian, A. Bulent, J. Hao, E. Jesse, J. B. Timothy, F. M. Charles, D. F. Mark, *Polymer* **2010**, 51.
[35] K. Hyeonjae, D. F. Mark, J. Hao, T. Scott, J. B. Timothy, F. M. Charles, *Polymer* **2004**, 45.
[36] R. F. Bunshah, *Handbook of Deposition Technologies for Films and Coatings: Science, Technology, and Applications*. Noyes Publications, Park Ridge, NJ **1994**.
[37] A. Nelson, *J. Appl. Crystallogr.* **2006**, *39*, 273.
[38] T. R. Gengenbach, R. C. Chatelier, H. J. Griesser, *Surf. Interface Anal.* **1996**, *24*, 271.
[39] T. R. Gengenbach, H. J. Griesser, *Polymer.* **1999**, *40*, 5079.
[40] A. Michelmore, P. M. Bryant, D. A. Steele, K. Vasilev, J. W. Bradley, R. D. Short, *Langmuir* **2011**, *27*, 11943.
[41] S. Lucas, G. Genard, C. Michiels, B. Masereel, O. Feron, B. Gallez, T. V. Borght, N. Moreau, *Nucl. Ins. Meth. Phys. Res. B* **2008**, 266.
[42] Y. Li, B. W. Muir, C. D. Easton, L. Thomsen, D. R. Nisbet, J. S. Forsythe, *Appl. Surf. Sci.* **2014**, 288.
[43] R. T. Chen, B. W. Muir, G. K. Such, A. Postma, R. A. Evans, S. M. Pereira, K. M. McLean, F. Caruso, *Langmuir* **2009**, *26*, 3388–3393.